PROCEEDINGS, 51st Workshop on Geothermal Reservoir Engineering
Stanford University, Stanford, California, February 9-11, 2026
SGP-TR-230

Concept of a High-Temperature EGS Plant in Central Oregon

Daniel W. Dichter, Trenton T. Cladouhos, Quinlan Byrne, Victor J. Rustom, and Greg Szutiak

20 University Road, Cambridge, MA

daniel.dichter@quaise.com, trenton.cladouhos@quaise.com, quinlan.byrne@quaise.com, victor.rustom@quaise.com, greg.szutiak@quaise.com

Keywords: EGS, enhanced, geothermal, high-temperature, Oregon, Newberry, fracture, reservoir, casing, erosion, steam, flash, cyclopentane, water-binary, ORC

ABSTRACT

Quaise, a geothermal development and drilling company, has broken ground on a high-temperature geothermal power plant in Central Oregon called Project Obsidian. It is sited outside of and adjacent to the southern boundary of the Newberry National Volcanic Monument. The geothermal gradient at the site is believed to be about 100 °C/km on the basis of nearby well temperature logs, and the targeted vertical depth range is about 4.3-4.9 km. The subsurface at this depth is expected to have very low natural permeability. Thereby, the project is expected to be completed by fracturing between wells using modern EGS (enhanced geothermal systems) techniques, rather than as a conventional hydrothermal project. Two reservoirs are planned, with targeted average feedzone temperatures of 315 °C and 365 °C. Each reservoir is to be connected to one injector well and two producer wells, with the wellfield comprising six flowing wells altogether. The injectors have a tie-back design with a 7” outer diameter casing throughout; the producers have a similar casing in the feedzone, stepping up to a 9 5/8” outer diameter casing around 2.5 km TVD to improve the flow characteristics of the more-compressible produced geofluid. The wells are planned to be inclined at 45° in the feedzone, to balance the challenges of directional drilling at high temperatures with the need for significant horizontality with which to connect the wells using vertical fracture planes. The geofluid enthalpy at the producer feedzones is considered as a key unknown, and a finite-element compressible flow model was developed to assess its significance, and its relation to geofluid pressure and phase. This model was used to generate a set of productivity curves, showing that liquid-dominated production and vapor-dominated production represent lower and upper bounds, respectively, for exergetic power at the wellheads. Several plant configurations were considered, including dry steam, flash, cyclopentane-binary, and water-binary. The best-performing cycle showed a strong dependence on the phase of the geofluid at the producer wellheads. Overall, it was found that the proposed system has the potential to deliver at least 50 MWe net from a total of six flowing wells using a binary cycle regardless of the geofluid phase.

1. SITE AND RESOURCE

Newberry Volcano – a large, active, shield-shaped stratovolcano 20 miles south of Bend, Oregon – has drawn researchers and developers to investigate its promising geothermal potential for 45 years. Exploration focused inside the caldera prior to establishment of the Newberry National Volcanic Monument in 1990, and on the northwest flank of the volcano since.

In 2025, Quaise acquired 1,334 acres of BLM geothermal leases on Newberry’s south flank, shown in Figure 1 on the following page. The geothermal gradient at the site is projected to be about 100 °C/km based on adjacent temperature core holes drilled in the 1980s, suggesting that rock temperatures above 300 °C can be reached at 3.5 km depth. These depths are expected to be relatively dry and impermeable. Recent magnetotelluric (MT), gravity, and passive seismic surveys, plus regional tectonic studies, have further validated the suitability of this site for EGS.

Four kilometers from the Quaise lease, the vent for the 1.3 thousand year old (ka) Big Obsidian Flow can be found along ring fractures that define the south rim of the caldera, indicating that the thermal anomaly may have recently shifted toward the Obsidian lease from the center of the caldera between the two lakes. Two geophysical anomalies are also present on the lease. A low seismic velocity anomaly, indicative of hotter rock, occurs 2.3 km below the leases. And a low-density anomaly, indicative of hotter rock or silica-rich intrusions into denser mafic rocks, trends across the southern rim. Lastly, a major regional fault zone, defined by the Walker Rim to the south and the Northwest Rift Zone to the north, passes through the Obsidian leases.

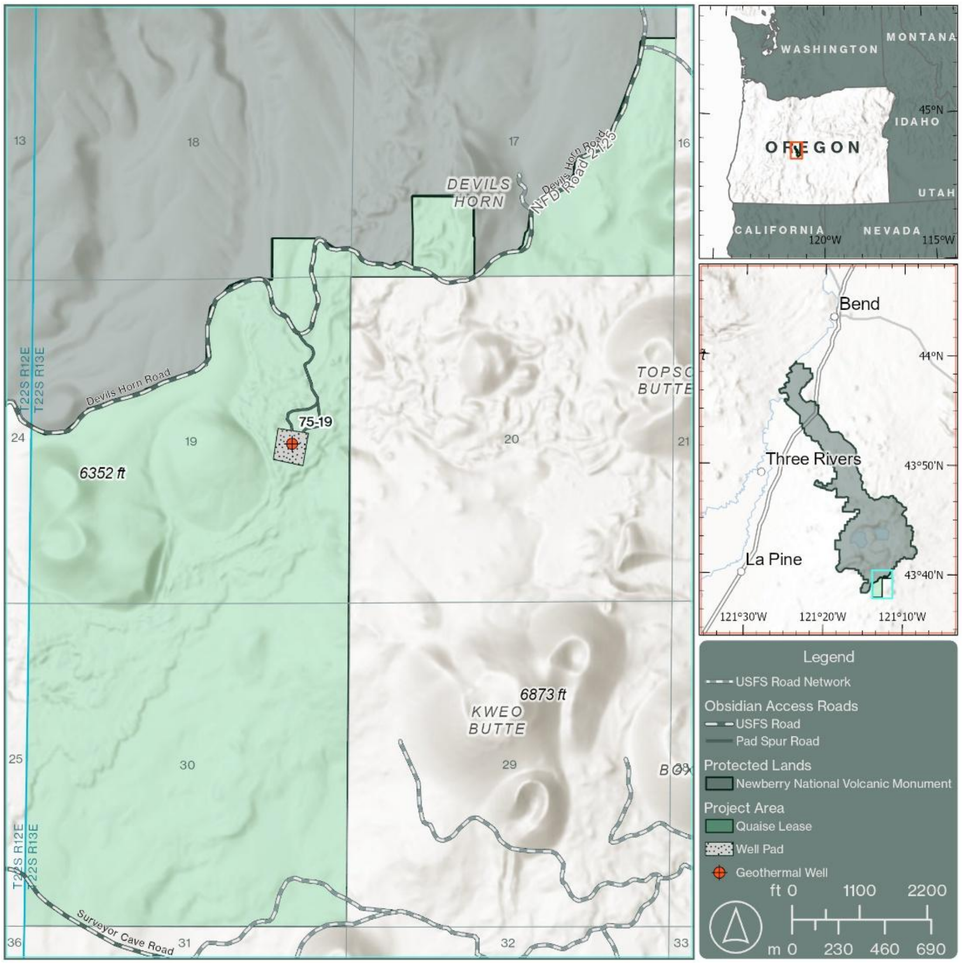

Figure 1: Map showing leased area and project site.

Climate data from a nearby weather station collected during a one-year period spanning 2015-2016 shows that the seasonal high air temperature ranges from about 30 °C in the summer to 10 °C in the winter. This is shown in Figure 2 below, and discussed further in Section 5 as a specification for power plant design.

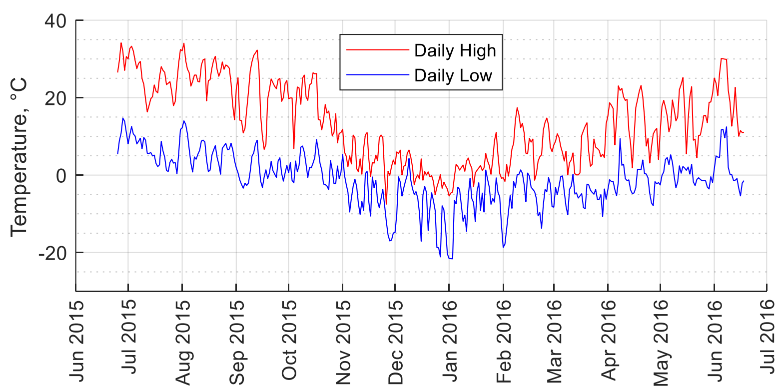

Figure 2: Daily air temperature highs and lows during a one-year period from 2015-2016 near the project site.

2. WELL SPECIFICATIONS

Quaise plans to develop two fractured reservoirs at this site, each serving one triplet consisting of one injector and two producers, for six flowing wells total. The target average feedzone temperatures for the two reservoirs are 315 °C and 365 °C. These correspond to feedzone temperature ranges of about 265-365 °C, and 315-415 °C, respectively, per the anticipated geothermal gradient described in Section 1. The planned trajectories and casing specifications for the producer wells are shown in Figure 3 below. The two producers associated with each reservoir are symmetrical about the east-west axis, such that each reservoir has a “north” producer, and a “south” producer, which are ideally interchangeable.

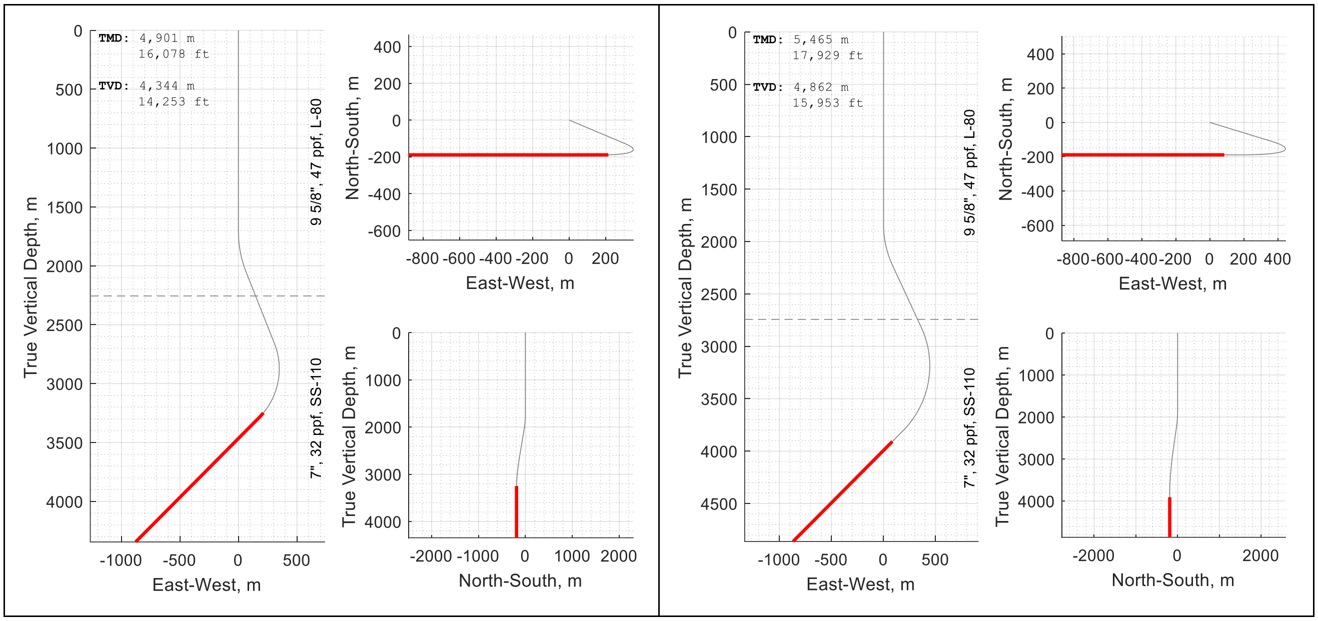

Figure 3: Side, top, and front views (clockwise from left) of the anticipated trajectories for the 315 °C (left) and 365 °C (right) producer wells, shown to scale in each subplot, and associated casing sizes. The feedzones are shown in red.

The wells are planned to be drilled vertically until reaching approximately 2 km TVD, after which they back-track slightly, then follow a straight path inclined at 45°. This inclination provides horizontality in the feedzone such that the wells can be connected by a series of fractures, which are expected to propagate approximately in the vertical direction. The chosen inclination angle may be modified within the approximate range of 45-80° based on confirmation well results, challenges associated with high-temperature directional drilling, and stimulation modeling. Regardless of the inclination angle, the trajectory is planned to provide a feedzone measuring at least 1 km long as projected onto the ground plane. The producer wells have a 7” outer diameter casing below about 2.5 km TVD, and a 9 5/8” outer diameter casing above; the injector wells have similar trajectories with a 7” outer diameter casing throughout.

3. FLOW MODEL

Geofluid within the producers is modeled as compressible, isenthalpic pipe flow using a one-dimensional finite-element method implemented in MATLAB, similar to commercial software WellSim. The geofluid is modeled as pure water. The individual elements are made sufficiently small that fluid flow within any single element can be treated as isochoric and incompressible. The pressure drop across a single element is described using the Darcy-Weisbach equation for frictional effects, and the hydrostatic equation for gravitational effects. The flow is assumed to be fully rough, a regime of turbulent flow in which the friction factor is independent of the Reynolds number. The friction factor is calculated using the von Kármán equation. These equations are shown below (Çengel et al., 2012).

$$\Delta P_{friction} = f\left(\frac{\Delta L}{D}\right)\left(\frac{\rho\, v^2}{2}\right) \tag{1}$$

$$\Delta P_{hydrostatic} = \rho\, g\, \Delta z \tag{2}$$

$$f = \left(-2.0\log\left(\frac{\epsilon/D}{3.7}\right)\right)^{-2} \tag{3}$$

Where f denotes the friction factor, ΔL denotes the element length, D denotes the element inner diameter, ρ denotes density, v denotes superficial flow velocity, g denotes gravitational acceleration, Δz denotes the element height in the vertical direction, and ϵ denotes the casing roughness, assumed as $\epsilon \approx 0.002$" [0.0046 mm] per commercial steel (Çengel et al., 2012). The cross-sectional flow area is considered to be variable with respect to the measured depth according to the casing designs shown in Figure 3.

The feedzone midpoint is considered as the flow inlet, and the wellhead is considered as the flow outlet. The temperature of the geofluid at the feedzone midpoint is assumed to be equal to the surrounding rock at that depth, i.e. 315 °C and 365 °C for the two reservoirs. That is, the geofluid is assumed to have a sufficiently long residence time in the reservoir that it reaches temperature equilibrium with the surrounding rock once it reaches the feedzone, and no short-circuited flow occurs.

The mass flow rate through the well is calculated numerically using the bisection method, starting at the feedzone midpoint and iterating upwards, such that the wellhead pressure resulting from the mass flow rate equals the commanded wellhead pressure. The individual elements are of equal length, in the sense of measured depth, at about 2 meters, per a mesh convergence study; i.e. each producer well is modeled as containing about 2,400-2,700 individual elements.

The maximum allowable erosional c-factor, as defined by API RP 14E, is tentatively taken as $c = 200$ (ft/s)(lb/ft^3)$^{1/2}$, corresponding to a solids-free and non-corrosive geofluid composition, to be confirmed by later circulation tests (API, 1991). Assuming that spent geofluid is reinjected in the liquid phase with a temperature no greater than 100 °C, the flow capacity through each injector is approximately 140 kg/s. This implies a mass flow rate capacity of about 60 kg/s per producer, allowing a margin of 20 kg/s due to leak-off at depth.

4. GEOFLUID PHASE

The primary unknown in the flow model described in Section 3 is the enthalpy of the geofluid at the feedzone midpoints of the producers, which is related to, but not strictly interchangeable with, its pressure or its phase, e.g. liquid, two-phase, vapor, etc. For example, water at 315 °C can range from compressed liquid at about 1,400 kJ/kg to superheated vapor at about 3,100 kJ/kg when unpressurized; at 365 °C, the range is similarly 1,625 kJ/kg to 3,200 kJ/kg. This is shown in Figure 4 below.

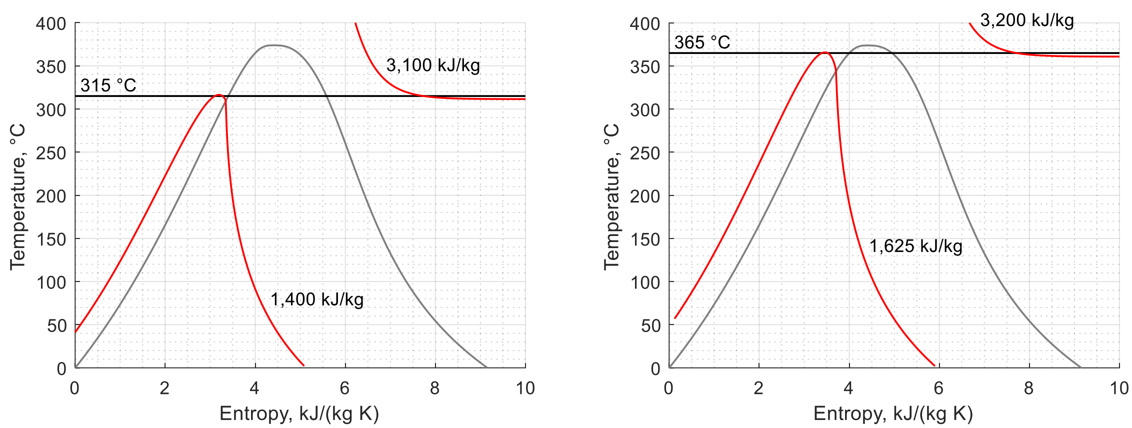

Figure 4: Approximate enthalpy ranges (red) for feedzone midpoint temperatures (black); phase boundary shown in gray.

For conventional hydrothermal geothermal reservoirs, the apparent reservoir pressure and enthalpy are essentially fixed quantities, and cannot be controlled directly, only influenced over long timescales via the balance of production and reinjection. Producer wells connected to such reservoirs have a certain optimal wellhead pressure, generally corresponding to that which maximizes the absolute or normalized output of the well, e.g. in units of MWe, or kWe/kg/s (DiPippo, 2016).

For example, the most recent datasheet from The Geysers shows that an average well has a depth of 2.6 km [8,500 ft] and produces 4.5 kg/s [36,083 lb/hr] of superheated steam at 185.9 °C [366.6 °F] and 6.6 bar [81.1 psig], yielding 1.94 MWe net per producer [5,471,562 net MWe-hr/1 year/322 wells] (Calpine, 2025). Assuming isenthalpic production and pure water, these conditions correspond to a reservoir enthalpy of about 2,815 kJ/kg. Representative plots for this type of well are shown in Figure 5 on the following page, using the flow model described in Section 3, assuming a casing design similar to those shown in Figure 3, albeit with a vertical rather than deviated trajectory.

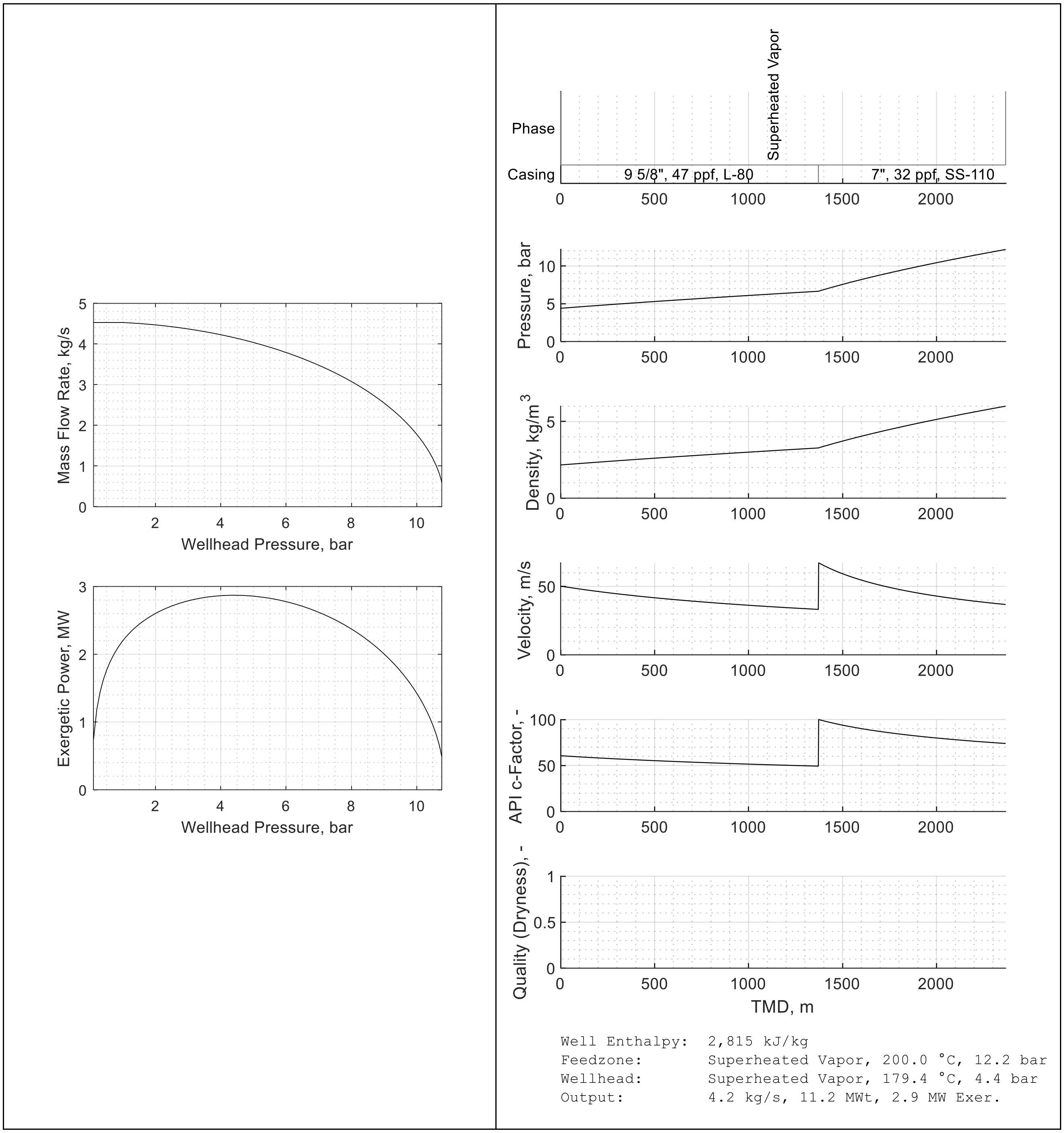

Figure 5: Productivity curves (left) and flow model (right) for a dry steam well similar to those at The Geysers.

The productivity curves (Figure 5, left) show that the maximum power output of the well occurs with a wellhead pressure between the limits of the well being fully open and shut in, conditions under which no power can be developed. This operating point (Figure 5, right) closely matches the reported flow characteristics described on the previous page.

For EGS reservoirs, production is more directly connected to injection, and thereby it may be possible to control the enthalpy of the geofluid at the producer feedzone to some extent via the wellhead pressures. For the wells proposed herein, this same process as shown in Figure 5 is repeated, taking the reservoir enthalpy as an additional independent parameter. Rather than yielding a single productivity curve, this yields a set of productivity curves for each well. The optimal design point is then selected from each curve, as described earlier, yielding the maximum exergetic power as a function of the reservoir enthalpy. This result is shown in Figure 6 below. For the purpose of calculating exergy, saturated liquid water at 30 °C is assumed as the dead state, per Sections 1 and 5.

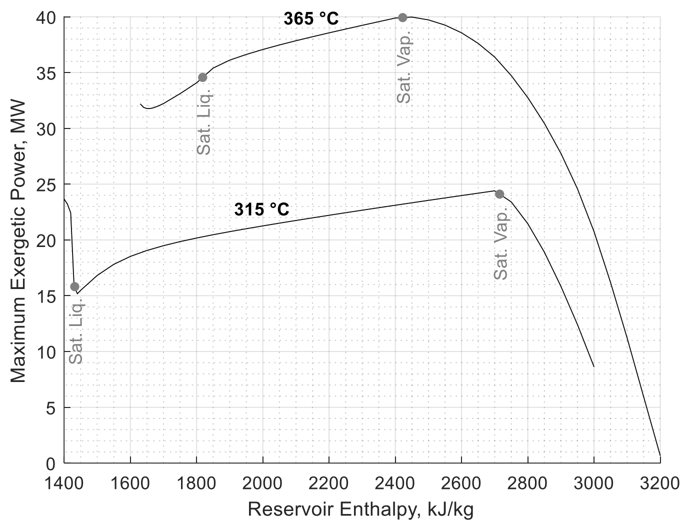

Figure 6: Maximum exergetic power as a function of mean feedzone temperature and enthalpy, such that $c \leq 200$ (ft/s)(lb/ft^3)$^{1/2}$.

Figure 6 shows that it is advantageous to avoid production of superheated steam, as the increased enthalpy is accompanied by a more substantial decrease in density and mass flow rate, overall causing a rapid decrease of exergetic power. It may also be advantageous to avoid production of compressed liquid, as this requires very high operating pressures throughout the gathering system and plant. These regimes can likely be avoided in operation by adjusting the injector and producer wellhead pressures.

Figure 6 also shows that outside of the compressed liquid and superheated steam regions, the maximum exergetic power increases as the reservoir enthalpy increases, for both reservoir temperatures. More specifically, the maximum exergetic power is approximately minimized with saturated liquid at the producer feedzone, and approximately maximized with saturated vapor at the producer feedzone. These flow scenarios are annotated in Figure 6 above, and detailed in Figures 7 and 8 on the following pages. It can be expected from Figure 6 that a two-phase mixture at the feedzone midpoint would attain an intermediate exergetic power between these two limiting cases.

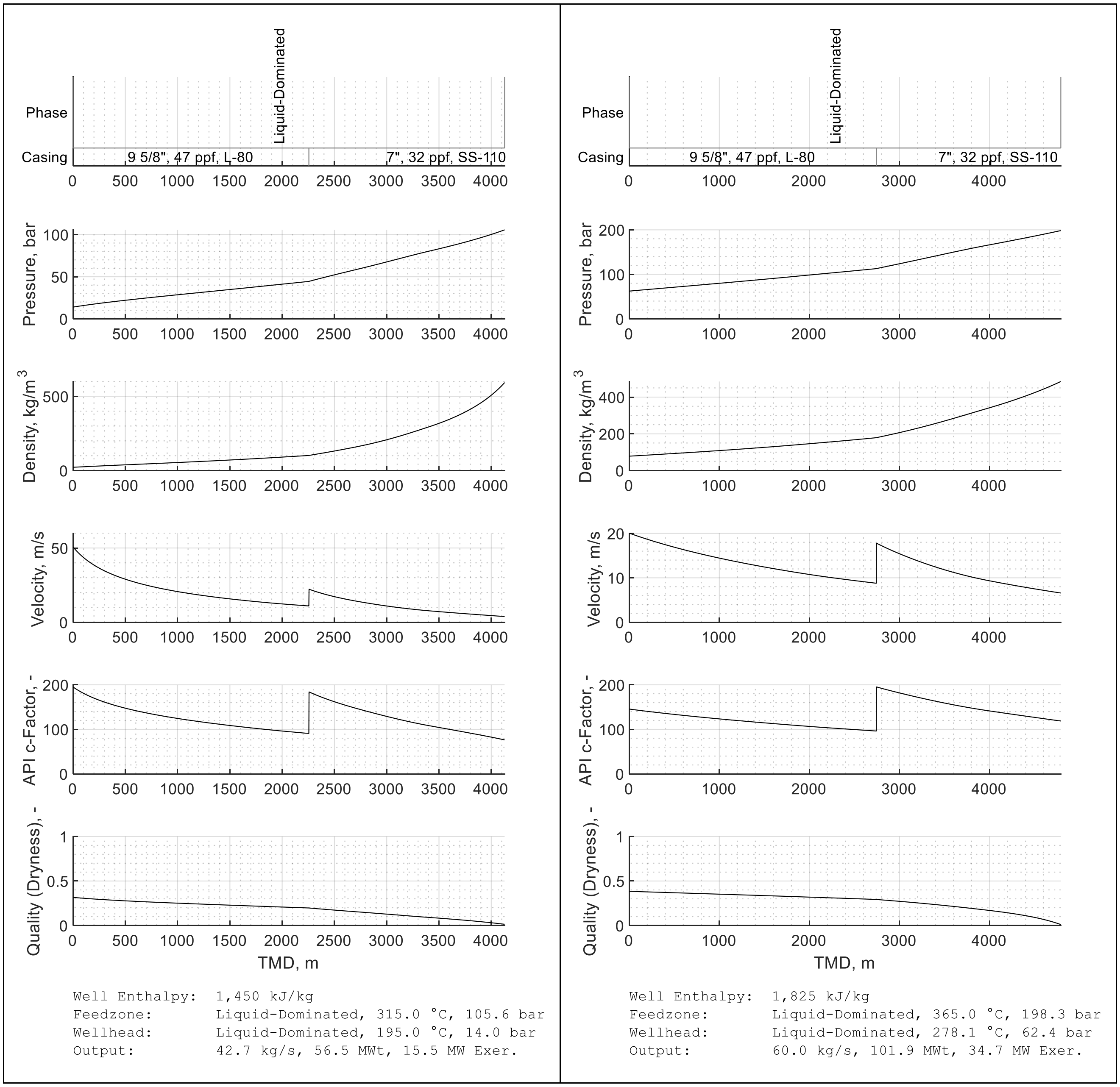

Figure 7: Production flow at 315 °C (left) and 365 °C (right) with saturated liquid at the feedzone.

Figure 7 shows that geofluid enters the producer well as a saturated liquid, and the subsequent depressurization as its flows upwards causes it to flash and progressively increase in quality. Geofluid reaches the wellheads with 30-40% quality. The larger casing size substantially reduces the flow velocity, increasing the flow capacity with respect to the erosional limit.

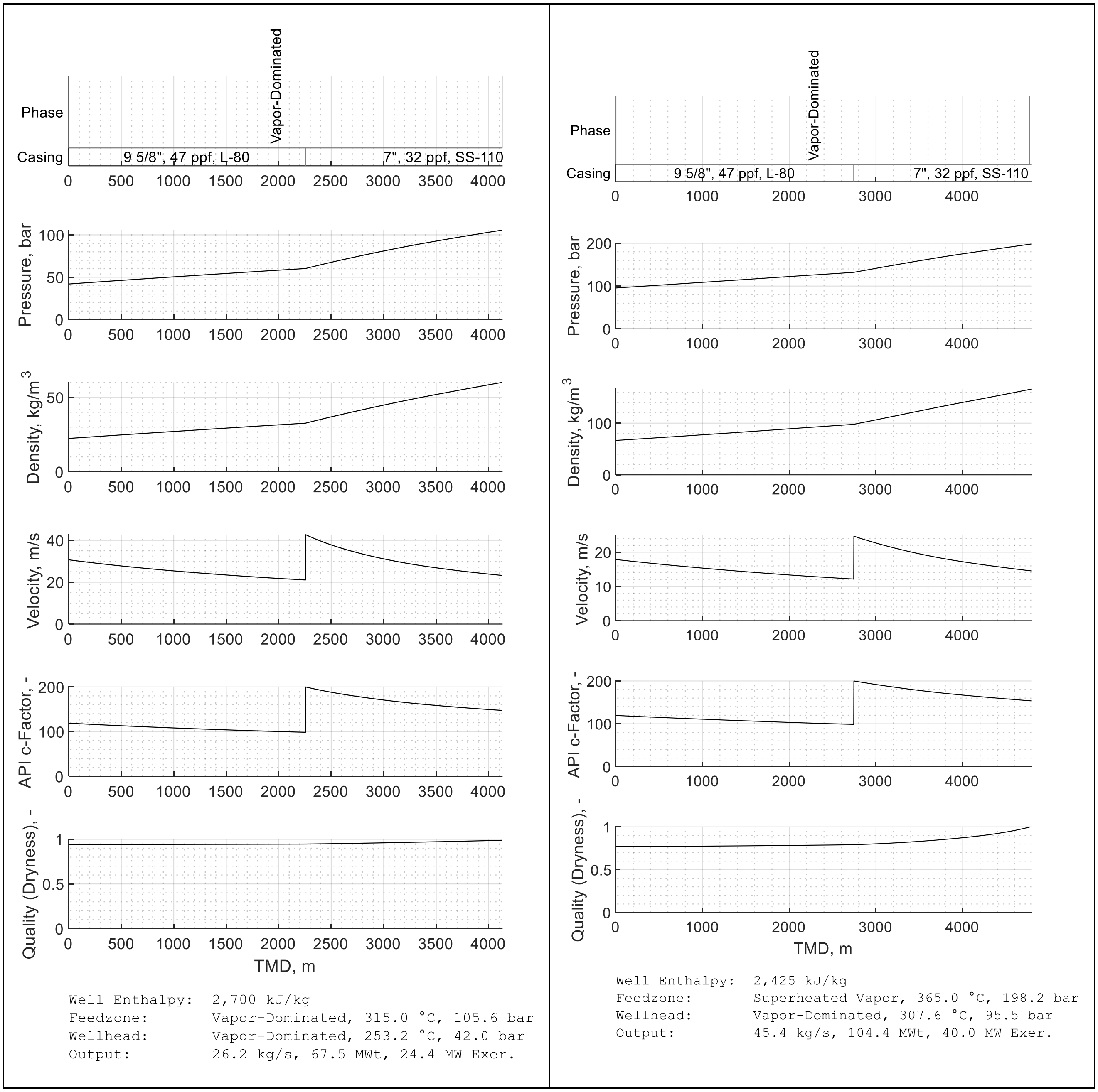

Figure 8: Production flow at 315 °C (left) and 365 °C (right) with saturated vapor at the feedzone.

Figure 8 shows that geofluid enters the producer well as a saturated vapor, and the subsequent depressurization as its flows upwards causes it to condense and progressively decrease in quality. Geofluid reaches the wellheads with 75-90% quality. The larger casing size improves flow capacity, though not as significantly as the liquid-dominated cases shown in Figure 7.

5. PLANT DESIGN

The plant is expected to be comprised of two co-located units: one dedicated to the 315 °C reservoir, and the other to 365 °C, so that each resource can be utilized most effectively. Three basic cycle types are considered: flash, cyclopentane-binary (a type of organic Rankine cycle, or ORC), and water-binary. With the relatively arid climate at the project site, an air-cooled condenser is anticipated. Its typical operating temperature is expected to be 30 °C, ± 10 °C due to seasonal temperature fluctuations, allowing a minimum temperature difference of 10 °C with respect to the ambient air temperature, as shown in Figure 2. In all cases, the turbine is assumed to have an 85% dry isentropic efficiency, the geofluid temperature kept above 100 °C to mitigate possible scaling and precipitation, and at least a 10 °C ΔT temperature difference, or pinch point, is maintained throughout all heat exchangers. For condensing (i.e. steam) turbines, the Baumann rule is applied, and a minimum quality or dryness of 85% is enforced (DiPippo, 2016). It can be shown that this minimum turbine quality precludes the use of a conventional dry steam cycle for the vapor-dominated cases shown in Figure 8; excessive condensation would occur. Gradient ascent is used to determine the set of cycle parameters that maximize exergetic efficiency, as described in previous work (Dichter, 2025). Future refinements of these cycles may include multiple vaporization pressures, feedwater heaters, and/or recuperators; these are not addressed in this work.

It was found that the cycle that confers the maximum gross power was a function of the geofluid production phase, rather than the feedzone temperature. Cyclopentane-binary was best suited for liquid-dominated production; water-binary for vapor-dominated production. These results are summarized in Table 1 below.

	Liquid-Dominated Prod.		**Vapor-Dominated Prod.**	
Cycle Type	**315 °C Feedzone**	**365 °C Feedzone**	**315 °C Feedzone**	**365 °C Feedzone**
Flash	5.4	14.3	11.6	17.3
Cyclopentane-Binary (ORC)	9.5	20.3	14.3	22.0
Water-Binary	8.1	18.1	15.2	24.8

Table 1: Optimized gross output per producer, MWe, vs. production phase, mean feedzone temperature, and cycle type.

Table 1 shows that the target feedzone temperatures are sufficiently hot that the two planned triplets have sufficient potential to produce the project's intended 50 MWe regardless of the geofluid's production phase, and whether cyclopentane or water is used as the plant's working fluid. The relatively poor performance of the flash cycle can be attributed to the constraint to not cool the geofluid below 100 °C; this does not similarly disadvantage the binary cycles because the secondary working fluid is allowed to reach 30 °C due to being chemically pure. The best-performing cycles are highlighted in Table 1 above and detailed in Figures 9 and 10 on the following pages.

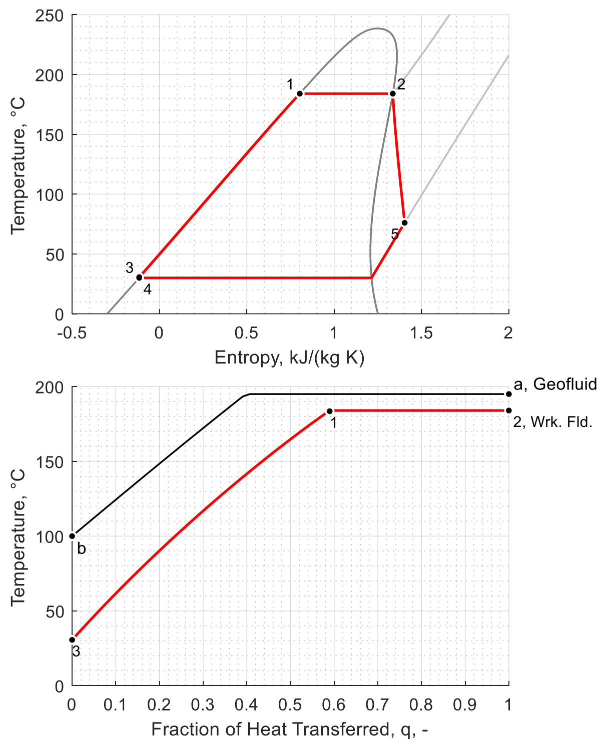

fluid	cyclopen	
q_in	593.4	kJ/kg
q_out	465.0	kJ/kg
w_net	128.4	kJ/kg
η_I	0.216	~
x_min	1.000	~

	T	P	h	s	x	m	ρ
	°C	bar	kJ/kg	kJ/(kg K)	-	-	kg/m^3
1	184.0	20.79	316.4	0.80	0.000	1.000	537.7
2	184.0	20.79	559.9	1.34	1.000	1.000	54.9
3	30.6	20.79	-33.5	-0.12	NaN	1.000	736.8
4	30.0	0.51	-36.2	-0.12	0.000	1.000	735.4
5	76.1	0.51	428.7	1.40	1.000	1.000	1.3

Geofluid		
Nominal Pressure	14.0	bar
Inlet Temperature	195.0	°C
Inlet Enthalpy	1450.0	kJ/kg
Outlet Temperature	100.0	°C
Outlet Enthalpy	420.4	kJ/kg
Mass Flow Rate	42.7	kg/s
Plant		
Mass Flow Rate (Wrk. Fld.)	74.1	kg/s
Turbine Stages	6	~
Last-Stage Blade Length	6.9	inch
Overall Turbine Diameter	0.9	m
Heat Input	44.0	MWt
Condenser Rejection	34.5	MWt
Gross Output	9.5	MWe
Utilization, η_II	0.614	~
Effectiveness	222.8	kWe/kg/s

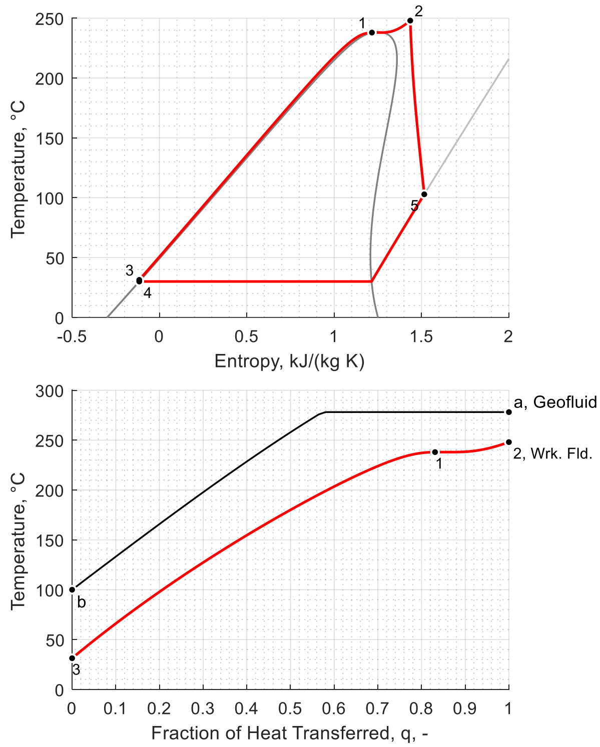

fluid	cyclopen	
q_in	666.2	kJ/kg
q_out	505.7	kJ/kg
w_net	160.6	kJ/kg
η_I	0.241	~
x_min	NaN	~

	T	P	h	s	x	m	ρ
	°C	bar	kJ/kg	kJ/(kg K)	-	-	kg/m^3
1	238.0	45.49	523.5	1.22	0.000	1.000	311.5
2	248.0	45.49	636.1	1.44	NaN	1.000	143.2
3	31.3	45.49	-30.1	-0.12	NaN	1.000	738.6
4	30.0	0.51	-36.2	-0.12	0.000	1.000	735.4
5	102.9	0.51	469.4	1.52	1.000	1.000	1.2

Geofluid		
Nominal Pressure	62.4	bar
Inlet Temperature	278.1	°C
Inlet Enthalpy	1825.0	kJ/kg
Outlet Temperature	100.0	°C
Outlet Enthalpy	424.0	kJ/kg
Mass Flow Rate	60.0	kg/s
Plant		
Mass Flow Rate (Wrk. Fld.)	126.2	kg/s
Turbine Stages	7	~
Last-Stage Blade Length	10.7	inch
Overall Turbine Diameter	1.0	m
Heat Input	84.1	MWt
Condenser Rejection	63.8	MWt
Gross Output	20.3	MWe
Utilization, η_II	0.585	~
Effectiveness	337.7	kWe/kg/s

Figure 9: Cyclopentane-binary cycles for liquid-dominated production from 315 °C (top) and 365 °C (bottom) feedzones.

For the 315 °C feedzone, a conventional single-pressure saturated cycle provides a good match between the cooling curves of the geofluid and working fluid. For the 365 °C feedzone, a small amount of superheating near the supercritical region, improves the cycle's performance, but it is still single-pressure.

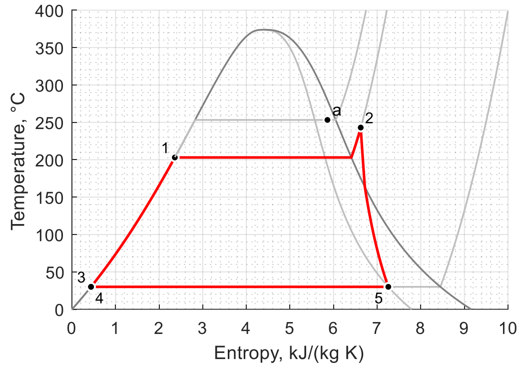

fluid	water
q_in	2773.0 kJ/kg
q_out	2067.3 kJ/kg
w_net	705.7 kJ/kg
η_I	0.254 ~
x_min	0.851 ~

	T	P	h	s	x	m	ρ
	°C	bar	kJ/kg	kJ/(kg K)	-	-	kg/m^3
1	203.0	16.57	866.0	2.36	0.000	1.000	861.1
2	243.0	16.57	2900.6	6.62	NaN	1.000	7.4
3	30.0	16.57	127.6	0.44	NaN	1.000	996.3
4	30.0	0.04	125.9	0.44	0.000	1.000	995.6
5	30.0	0.04	2193.3	7.26	0.851	1.000	0.0

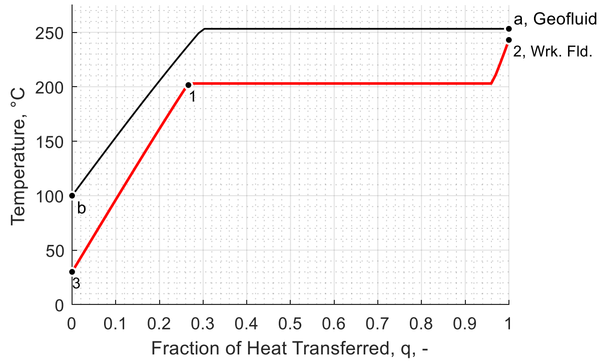

Geofluid

Nominal Pressure	42.0	bar
Inlet Temperature	253.2	°C
Inlet Enthalpy	2700.0	kJ/kg
Outlet Temperature	100.0	°C
Outlet Enthalpy	422.5	kJ/kg
Mass Flow Rate	26.2	kg/s

Plant

Mass Flow Rate (Wrk. Fld.)	21.5	kg/s
Turbine Stages	8	~
Last-Stage Blade Length	24.6	inch
Overall Turbine Diameter	1.7	m
Heat Input	59.7	MWt
Condenser Rejection	44.5	MWt
Gross Output	15.2	MWe
Utilization, η_II	0.623	~
Effectiveness	579.6	kWe/kg/s

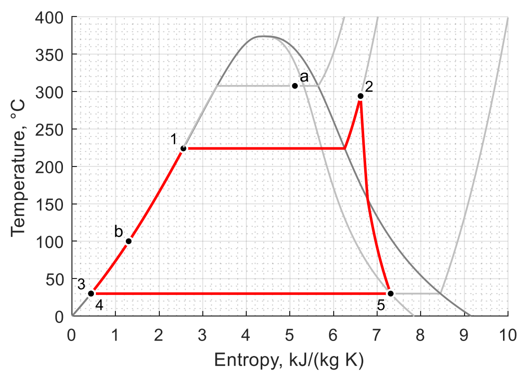

fluid	water
q_in	2866.5 kJ/kg
q_out	2083.7 kJ/kg
w_net	782.8 kJ/kg
η_I	0.273 ~
x_min	0.858 ~

	T	P	h	s	x	m	ρ
	°C	bar	kJ/kg	kJ/(kg K)	-	-	kg/m^3
1	224.0	25.05	962.4	2.56	0.000	1.000	835.0
2	294.0	25.05	2994.9	6.62	NaN	1.000	10.3
3	30.1	25.05	128.5	0.44	NaN	1.000	996.7
4	30.0	0.04	125.9	0.44	0.000	1.000	995.6
5	30.0	0.04	2209.6	7.31	0.858	1.000	0.0

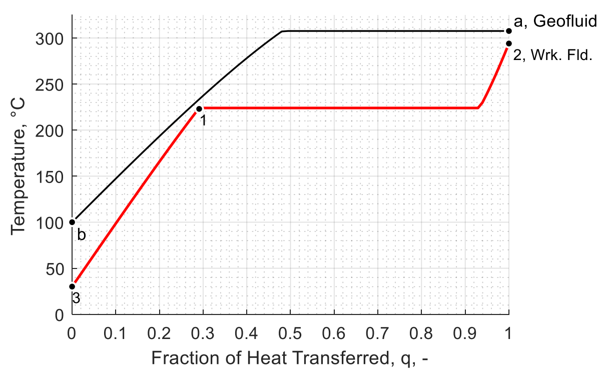

Geofluid

Nominal Pressure	95.5	bar
Inlet Temperature	307.6	°C
Inlet Enthalpy	2425.0	kJ/kg
Outlet Temperature	100.0	°C
Outlet Enthalpy	426.5	kJ/kg
Mass Flow Rate	45.4	kg/s

Plant

Mass Flow Rate (Wrk. Fld.)	31.7	kg/s
Turbine Stages	9	~
Last-Stage Blade Length	31.5	inch
Overall Turbine Diameter	2.1	m
Heat Input	90.7	MWt
Condenser Rejection	66.0	MWt
Gross Output	24.8	MWe
Utilization, η_II	0.619	~
Effectiveness	545.8	kWe/kg/s

Figure 10: Water-binary cycles for vapor-dominated production from 315 °C (top) and 365 °C (bottom) feedzones.

For both the 315 °C and 365 °C cases, it is advantageous to superheat the working fluid before the turbine; the magnitude increases for the latter case. Introducing a second vaporization pressure confers only a marginal improvement to the gross power.

6. PROJECT OUTLOOK

Road and pad work is nearly complete, as shown in Figure 11. Other ongoing activities include timber processing, rock crushing, and sump excavation. The pad measures 450 feet by 400 feet, and will eventually host seven wells and a gathering system. In Q2 2026, a deep confirmation well will be drilled to provide the data needed to design, drill, and develop EGS wells at the site. Data collected will include the temperature profile at near-reservoir depth, minimum horizontal principal stress magnitude and orientation, rock type, hydrothermal alteration, deep intrusions, and presence of native permeability and geothermal fluids. After open-hole logging, this well will be completed as a monitoring and fracture test well with installation of casing, fiber-optic cable, and stimulation sleeves. In Q3 and Q4 2026, the first well pair will be drilled and stimulated with the goal of performing a circulation test by the end of the year. The project is intended to deliver power as early as 2030.

In addition to drilling, magnetotelluric data collected in Q4 2025 is currently being processed, and will provide characteristics (e.g. strike, dip, extent, and thickness) of large local structures – fault zones, fault offsets, alteration zones, and clay caps. Passive microseismic monitoring will inform induced seismicity risk evaluation and locate critically stressed fractures that may host native fluids.

In parallel with the field work, Quaise is refining fracturing and reservoir models, and supporting laboratory testing. Modeling will help develop reservoir stimulation plans so as to achieve acceptable performance in both initial and long-term capacities, including parameters such as the fracture quantity, spacing, and size, and how these relate to the reservoir's effective surface area and effective volume. Laboratory testing will be used to help select proppants and zonal isolation equipment suitable for the extreme conditions that will be encountered in the planned wells.

Figure 11: Road and pad at Project Obsidian as of January 2026, with artist's rendering of completed plant.

7. SUMMARY

This paper provided an overview of Quaise's planned 50 MWe geothermal power plant located outside the southern boundary of the Newberry National Volcanic Monument in Central Oregon, called Project Obsidian. The geothermal gradient at this site is expected to be relatively high, at about 100 °C/km. Two triplet reservoirs are planned, with target mean feedzone temperatures of 315 °C and 365 °C. The climate at this site is relatively cool and arid, with daily highs of typically 20 °C ± 10 °C, which is favorable for heat rejection and plant performance, and will likely require the use of an air-cooled condenser.

The wells are planned to be drilled vertically for about the first 2 km of depth, after which they back-track slightly, then follow a straight path inclined at 45°. This inclination angle may be modified within the approximate range of 45-80° based on confirmation well results, challenges associated with high-temperature directional drilling, and stimulation modeling, such that the horizontal extent of the feedzones remains at least 1 km long. The wells are to be connected by a series of vertical planar fractures. The producer wells have a 7" outer diameter casing below about 2.5 km TVD, and a 9 5/8" outer diameter casing above; the injector wells have a 7" outer diameter casing throughout.

A one-dimensional finite-element model was developed for compressible isenthalpic flow along these well trajectories with a variable casing size. This accounted for both frictional and hydrostatic effects using standard equations. The midpoint of the feedzone was considered as the flow inlet, and the wellhead as the flow outlet. The geofluid was assumed to be in temperature equilibrium with the surrounding rock once reaching the producer feedzone. Erosion was considered as the limiting factor on the flow rates within the wells; the de facto standard of API RP 14E was used with a c-factor of 200 (ft/s)(lb/ft^3)$^{1/2}$, tentatively assuming the produced geofluid is solids-free and non-corrosive.

The enthalpy of the geofluid at the producer feedzones was considered as a key unknown due to its dependence on geological factors and the outcomes of forthcoming stimulation work. This is critically related to both its pressure and phase. An example was given of how productivity curves can be used to determine the optimal wellhead pressure for a reservoir of a certain enthalpy. For the system considered herein, the full ranges of possible enthalpies were considered, showing that the optimized exergetic power is minimized with saturated liquid at the feedzone midpoint, and maximized with saturated vapor at the feedzone midpoint, though both scenarios show significant potential. With saturated liquid at the feedzone, the geofluid flashes as it exits the reservoir and progressively increases in quality, or dryness, as it flows upwards; the opposite occurs with saturated vapor. Scenarios involving compressed liquid were excluded from consideration for requiring system pressures that are likely excessive, and superheated vapor was found to confer lower exergetic power because of its relatively low density and mass flow rate. The use of a variable-size casing was shown to substantially increase the flow capacity of the producer wells as compared to a tie-back design with a single casing size.

Flash, cyclopentane-binary (i.e. ORC), and water-binary cycles were considered to convert the heat of the produced geofluid to electrical power. Liquid-dominated production favors a cyclopentane-binary cycle, with a saturated cycle for the 315 °C reservoir, and a slightly superheated or slightly supercritical cycle for the 365 °C reservoir. Vapor-dominated production favors a water-binary cycle, with single-pressure superheated cycles for both reservoir temperatures. Multiple vaporization pressures, feedwater heaters, and/or recuperators were noted as possible refinements of these cycles. Regardless of whether production is liquid-dominated or vapor-dominated, and whether a cyclopentane-binary or water-binary cycle is used, the two triplets showed a total potential exceeding the target of 50 MWe.

Road and pad development is nearly complete, with drilling, stimulation, and circulation planned throughout 2026, and a goal of delivering power as early as 2030.

REFERENCES

American Petroleum Institute (API): Recommended Practice for Design and Installation of Offshore Production Platform Piping Systems, RP 14E, Washington, D.C. (1991).

Calpine: The Geysers Geothermal Field 2024 Statistics, <https://geysers.com/wp-content/uploads/2025/08/2025-The-Geysers-by-the-Numbers-AV.pdf>, (2025).

Çengel, Y.A., Cimbala, J.M., and Turner, R.H.: Fundamentals of Thermal-Fluid Sciences, McGraw-Hill, 4th edition, (2012).

Dichter, D.: Water-Based Geothermal Binary Cycles, Proceedings, 50th Workshop on Geothermal Reservoir Engineering, Stanford University, Stanford, CA (2025).

DiPippo, R.: Geothermal Power Plants, Butterworth-Heinemann, 4th edition, (2016).

Lemmon, E.W., et al.: NIST Standard Reference Database 23: Reference Fluid Thermodynamic and Transport Properties-REFPROP, Version 10.0, National Institute of Standards and Technology, (2018).